

# The Structural Basis of Riboflavin Binding to *Schizosaccharomyces pombe* 6,7-Dimethyl-8-ribityllumazine Synthase

Stefan Gerhardt<sup>1\*</sup>, Ilka Haase<sup>2</sup>, Stefan Steinbacher<sup>1</sup>, Jens T. Kaiser<sup>1</sup>  
Mark Cushman<sup>3</sup>, Adelbert Bacher<sup>2</sup>, Robert Huber<sup>1</sup> and Markus Fischer<sup>2\*</sup>

<sup>1</sup>Max-Planck-Institut für Biochemie, Abteilung Strukturforschung  
Am Klopferspitz 18a, D-82152 Martinsried, Germany

<sup>2</sup>Lehrstuhl für Organische Chemie und Biochemie Technische Universität München, Lichtenbergstr. 4 D-85747 Garching, Germany

<sup>3</sup>Department of Medicinal Chemistry and Molecular Pharmacology, Purdue University, West Lafayette IN 47907, USA

Riboflavin is an essential cofactor in all organisms. Its direct biosynthetic precursor, 6,7-dimethyl-8-ribityllumazine, is synthesised by the enzyme 6,7-dimethyl-8-ribityllumazine synthase. Recently, we have found that the enzyme from *Schizosaccharomyces pombe* binds riboflavin, the final product of the pathway with a relatively high affinity with a  $K_D$  of 1.2  $\mu$ M.

Here, we report on the crystal structure of lumazine synthase from *S. pombe* with bound riboflavin and compare the binding mode with those of the substrate analogue inhibitor 5-nitro-6-(D-ribitylamino)-2,4(1H,3H)-pyrimidinedione and of the product analogue 6-carboxyethyl-7-oxo-8-ribityllumazine. In all complexes the pyrimidinedione moieties of each respective ligand bind in a very similar orientation. Binding of riboflavin additionally involves a stacking interaction of the dimethylbenzene moiety with the side-chain of His94, a highly conserved residue in all lumazine synthases. The enzyme from *Bacillus subtilis* showed a  $K_D$  of at least 1 mM whereas the very homologous enzyme from *Saccharomyces cerevisiae* had a comparable  $K_D$  of 3.9  $\mu$ M. Structural comparison of the *S. cerevisiae*, the *S. pombe*, and the mutant enzymes suggests that fine tuning of affinity is achieved by influencing this stacking interaction.

© 2002 Elsevier Science Ltd. All rights reserved

**Keywords:** riboflavin biosynthesis; lumazine synthase; crystal structure; *Schizosaccharomyces pombe*; ligand binding

\*Corresponding authors

## Introduction

The xylene ring of the vitamin, riboflavin, is assembled from two molecules of 3,4-dihydroxy-2-butanone 4-phosphate (**2**) in two consecutive steps (Figure 1).<sup>1–6</sup> Initially, **2** condenses with 5-amino-6-(D-ribitylamino)-2,4(1H,3H)-pyrimidinedione (**1**) to form 6,7-dimethyl-8-ribityllumazine (**3**). The product **3** undergoes an unusual dismutation reaction resulting in formation of one equivalent of riboflavin (**4**) accompanied by the regeneration of one equivalent of **1**.

The condensation of the carbohydrate derivative **2** with **1** is catalysed by lumazine synthase. The

enzyme-catalysed reaction is assumed to begin with the formation of a Schiff base (**5**) between the carbonyl group of **2** and the 5-amino group of **1**. Following the elimination of inorganic phosphate from the intermediate, the pyrazine ring of **6** can be closed by a nucleophilic attack of the position 6 amino group of intermediate **7** on the position 5 side-chain (Figure 2).

The structure of lumazine synthases has been studied in some detail. The enzymes from *Bacillus subtilis*,<sup>7–12</sup> *Aquifex aeolicus*,<sup>13</sup> *Escherichia coli*<sup>14</sup> and spinach<sup>15</sup> form icosahedral capsids comprising 60 identical subunits which are best described as dodecamers of pentamers. The icosahedral capsids of *B. subtilis* as well as of other Bacillaceae enclose homotrimeric riboflavin synthase in the core space.<sup>7,8</sup> This unusual topology is conducive to substrate channelling resulting in enhanced catalytic efficiency at low substrate concentration.<sup>6</sup>

More recently, the lumazine synthases from *S. cerevisiae*,<sup>16</sup> *Magnaporthe grisea*<sup>15</sup> and *Brucella*

Abbreviations used: RIBO, riboflavin-bound lumazine synthase; NRAP, 5-nitro-6-(D-ribitylamino)-2,4(1H,3H)-pyrimidinedione; CEOL, 6-carboxyethyl-7-oxo-8-ribityllumazine; PDB, protein data base.

E-mail addresses of the corresponding authors: gerhardt@biochem.mpg.de; markus.fischer@ch.tum.de

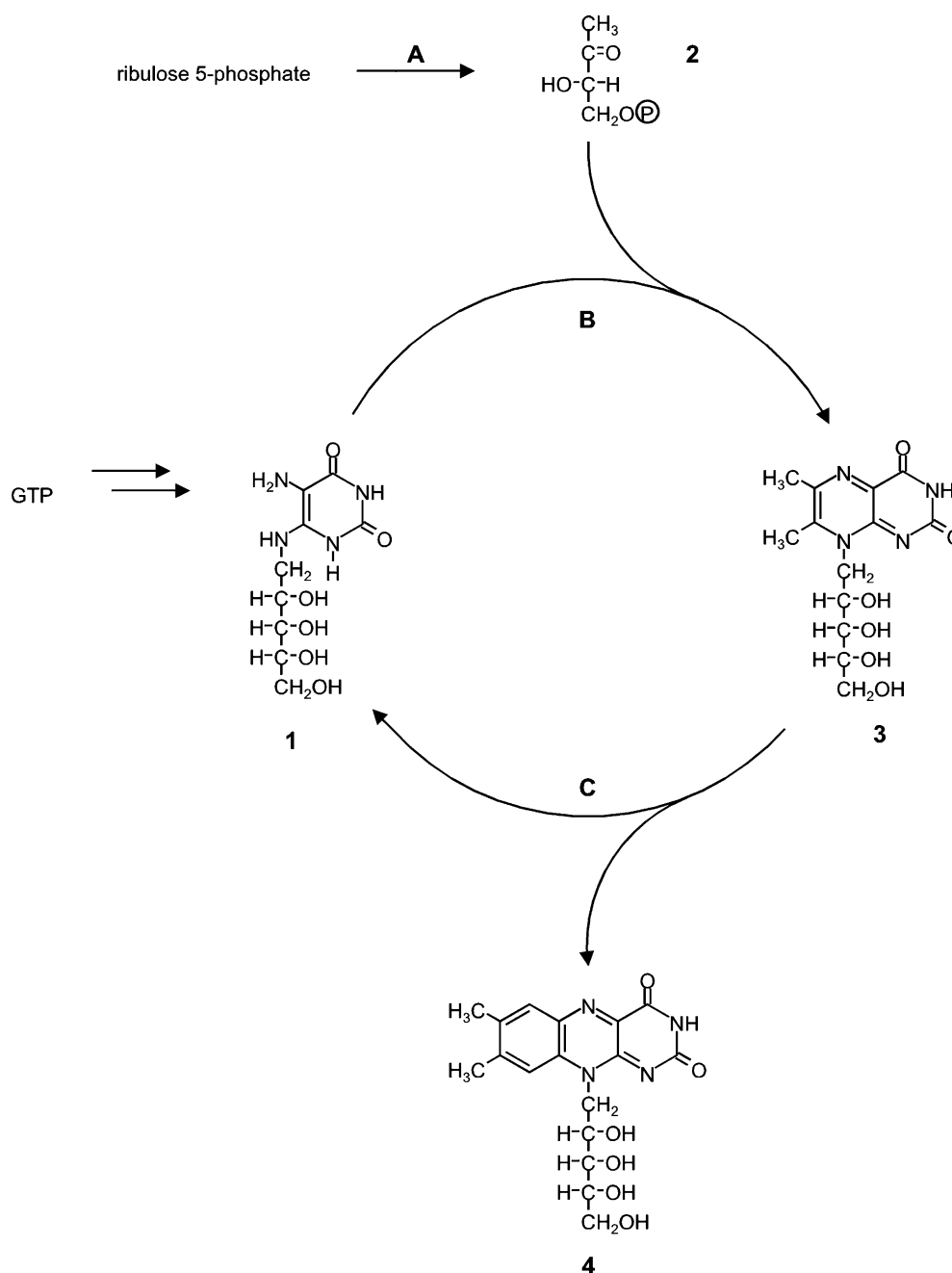


**Figure 1.** Terminal reactions in the pathway of riboflavin biosynthesis. (a) 3,4-Dihydroxy-2-butanone 4-phosphate synthase; (b) 6,7-dimethyl-8-ribityllumazine synthase; (c) riboflavin synthase.

*abortus*<sup>17</sup> have been found to be homopentamers whose topology is closely similar to that of the pentameric modules in the icosahedral enzymes. In all lumazine synthases studied, the topologically equivalent active sites are located at the interfaces between adjacent subunits in the pentameric modules.

Pathogenic enterobacteria<sup>18</sup> and probably pathogenic yeasts<sup>19,20</sup> are unable to incorporate riboflavin from the environment and are therefore absolutely dependent on endogenous synthesis of the vitamin. Recent genomic studies suggest that the riboflavin pathway is also essential for

*Mycobacterium tuberculosis* and *Mycobacterium leprae*. Therefore, the enzymes of the riboflavin biosynthetic pathways represent potential targets for anti-bacterial and anti-fungal agents.

Recently, we have found that recombinant lumazine synthase from *Schizosaccharomyces pombe* is isolated with bound riboflavin, the final product of the biosynthetic pathway. The relatively high affinity of the *S. pombe* enzyme is indicated by a  $K_D$  of 1.2  $\mu\text{M}$ . Complete extraction of riboflavin from such preparations could only be achieved by denaturation of the protein with urea.<sup>21</sup> In contrast, all other lumazine synthases studied so far were

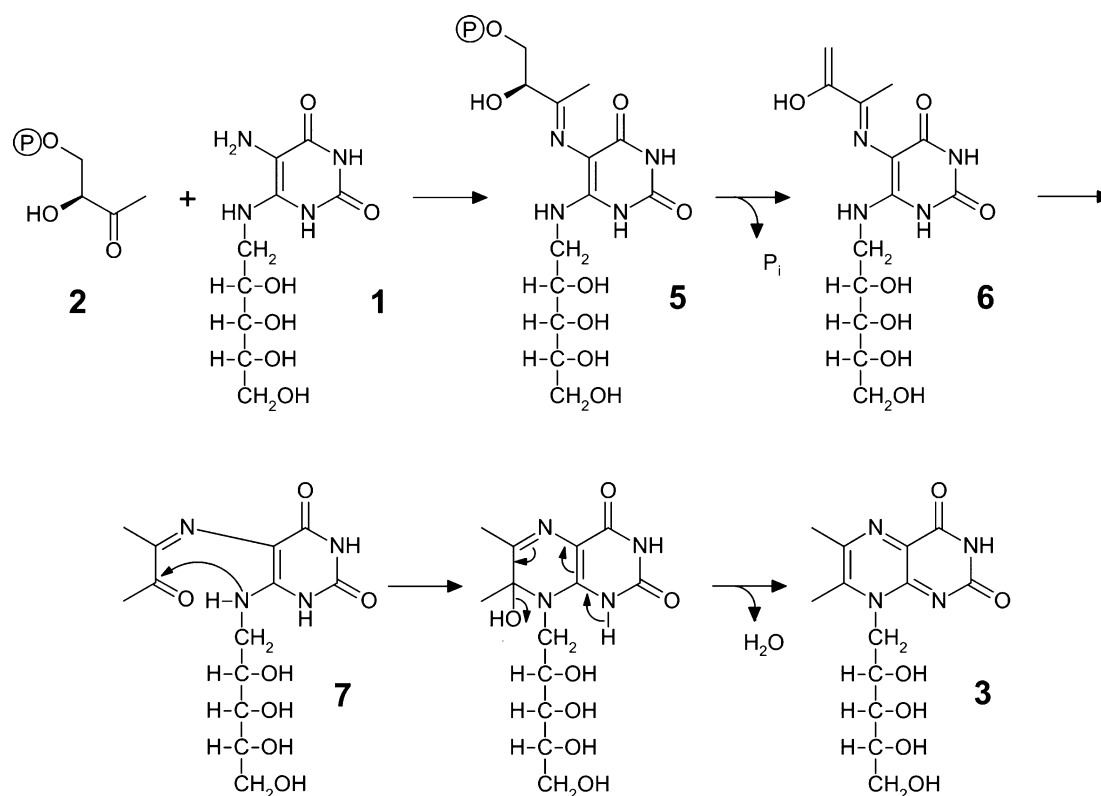


Figure 2. Hypothetical reaction mechanism of 6,7-dimethyl-8-ribityllumazine synthase.<sup>5</sup>

isolated without bound riboflavin, indicating a significantly lower affinity. This unexpected property of the *S. pombe* enzyme prompted us to determine its three-dimensional structure which is reported here. In addition we have measured the affinity of lumazine synthases from *B. subtilis* and *S. cerevisiae* for riboflavin. Our results suggest that efficient stacking of the dimethylbenzene moiety of riboflavin with the highly conserved His94 is a major determinant of affinity. However, it is unclear at the moment whether this property is used as a feedback regulation mechanism of riboflavin biosynthesis in yeasts.

## Results and Discussion

### Quality of the models

Lumazine synthase from *S. pombe* was crystallised either in complex with bound riboflavin (4) as isolated from recombinant *E. coli* (RIBO) or in complex with the substrate analogue 5-nitro-6-(D-ribitylamino)-2,4(1*H*,3*H*)-pyrimidinedione (NRAP) (8) or the product analogue 6-carboxyethyl-7-oxo-8-ribityllumazine (CEOL) (9) (Figure 3). The mutant proteins W27G, W63Y and W63Y/L119F, which do not bind riboflavin, and the mutant L119F, which only weakly binds to riboflavin, were also analysed. Diffraction data were collected to resolutions of 2.4 Å (RIBO), 2.4 Å (NRAP), 2.6 Å (CEOL), 2.0 Å (W27G), 3.1 Å (W63Y and L119F) and 2.7 Å (W63Y/L119F), respectively. All crystals

belongs to space group C222<sub>1</sub> with one pentamer in the asymmetric unit corresponding to the solution state of the protein. The crystal structure in complex with riboflavin was solved by Patterson search techniques using a pentameric facet from the icosahedral capsid of the *B. subtilis* lumazine synthase.<sup>12</sup> The resulting refined model was used to analyse the other *S. pombe* lumazine synthase complexes and mutants. The structures were refined to crystallographic *R* values of 18.0% (*R*<sub>free</sub> = 21.3%) (RIBO), 18.3% (*R*<sub>free</sub> = 21.3%) (NRAP), 17.5% (*R*<sub>free</sub> = 20.6%) (CEOL), 18.7% (*R*<sub>free</sub> = 21.2%) (W27G), 19.4% (*R*<sub>free</sub> = 23.2%) (W63Y), 19.4% (*R*<sub>free</sub> = 23.1%) (L119F), 19.2% (*R*<sub>free</sub> = 22.5%) (W63Y/L119F) with good stereochemistry (Table 1). More than 95% of all residues were found in the most favoured region of the

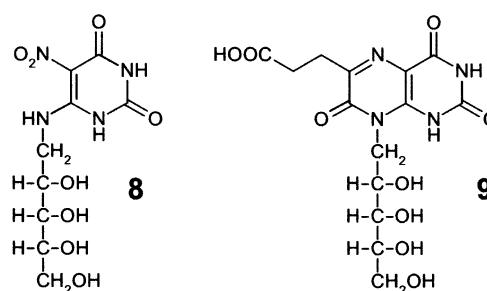


Figure 3. Inhibitors of 6,7-dimethyl-8-ribityllumazine synthase.

**Table 1.** X-ray data-processing and final refinement statistics

	Complexes				Mutants		
	RIBO	NRAP	CEOL	W27G	W63Y	L119F	W63Y/L119F
Cell constants (Å)							
<i>a</i>	111.50	111.26	111.09	110.57	111.94	111.76	111.52
<i>b</i>	145.52	145.04	145.18	144.02	145.92	145.50	145.38
<i>c</i>	128.70	127.86	128.55	126.36	129.28	129.13	129.12
Space group	C222 <sub>1</sub>						
Resolution limit (Å)	2.4	2.4	2.6	2.0	3.1	3.1	2.7
Reflections, unique	40,966	39,592	32,116	66,756	19,153	18,896	28,373
Multiplicity	3.5	2.9	3.7	3.8	2.6	3.5	2.9
$R_{\text{merge}}^{\text{a}}$ overall	0.078	0.079	0.07	0.051	0.11	0.12	0.077
$R_{\text{merge}}^{\text{b}}$	0.45	0.41	0.42	0.75	0.34	0.36	0.37
Completeness overall (%)	99.5	97.6	99.5	98.0	98.6	97.7	98.0
Completeness (%) <sup>b</sup>	99.5	97.6	99.5	98.0	99.9	99.2	100.0
Non hydrogen protein atoms	5695	5713	5700	5677	5640	5665	5655
Solvent molecules	94	127	45	205	77	66	89
Non hydrogen ligand atoms	135	105	135	–	–	–	–
Non hydrogen ion atoms	25	25	25	–	25	25	25
Resolution range (Å)	16.03–2.4	15.6–2.4	15.46–2.6	20.0–2.0	30.4–3.1	24.18–3.1	30.86–2.7
$R_{\text{value}}$ overall <sup>c</sup> (%)	18.0	18.3	17.5	18.7	19.4	19.4	19.2
$R_{\text{free}}^{\text{d}}$ (%)	21.3	21.3	20.6	21.2	23.2	23.1	22.5
r.m.s. standard deviations							
Bond lengths (Å)	0.012	0.009	0.009	0.012	0.008	0.008	0.007
Bond angles (°)	1.75	1.43	1.44	1.59	1.35	1.35	1.36
Average <i>B</i> -values/SD (Å <sup>2</sup> )							
Protein	44.2	43.9	46.1	40.7	30.4	28.7	38.8
Ligand	61.7	37.8	45.9	–	–	–	–
Solvent	48.7	49.2	45.9	47.4	35.1	29.4	34.4
Ion	49.8	39.8	55.6	–	35.4	30.7	42.9

<sup>a</sup>  $R_{\text{merge}} = \sum_{hkl} [(\sum_i |I_i - \langle I \rangle|) / \sum_i I_i]$ .

<sup>b</sup> Values correspond to the highest resolution shell (RIBO: 2.53–2.4 Å; NRAP: 2.53–2.4 Å; CEOL: 2.74–2.6 Å; W27G: 2.03–2.0 Å; W63Y: 3.27–3.1 Å; L119F: 3.27–3.1 Å; W63Y/L119F: 2.85–2.7 Å).

<sup>c</sup>  $R_{\text{value}} = \sum_{hkl} |F_{\text{obs}} - F_{\text{calc}}| / \sum_{hkl} F_{\text{obs}}$ .

<sup>d</sup>  $R_{\text{free}}$  is the cross-validation *R* factor computed for the test set of 10% of unique reflections.

Ramachandran plot in all structures described here (Table 2).

The monomers of *S. pombe* lumazine synthase (Figure 4) consist of 159 residues that were well defined in all structures with the exception of the first 11 residues. The latter were disordered to various extents in different subunits whereas the C-terminal residue Tyr159 was disordered in all subunits. Most of the side-chains were clearly defined by their electron density map, except for some located at the surface of the protein. The final model of the wild-type pentamer (Figure 5) is comprised of 742 amino acid residues in total. A

well-defined phosphate ion is found in all subunits in the putative binding site of the second substrate, 3,4-dihydroxy-2-butanone 4-phosphate (2), in those complexes that were crystallised in the presence of high phosphate concentrations, i.e. all with the exception of RIBO.

The temperature factors of riboflavin (61.7 Å<sup>2</sup>) are higher than the average temperature factors of the protein (44.2 Å<sup>2</sup>), whereas those of the inhibitors 8 and 9 are in the same range as the protein, reflecting the somewhat lower affinity of riboflavin to the protein (Table 1). However, all ligands were well-defined in the final electron density maps (Figure 6).

**Table 2.** Final Ramachandran statistics/ $\Phi$ ,  $\Psi$  angle distribution

	Complexes				Mutants		
	RIBO	NRAP	CEOL	W27G	W63Y	L119F	W63Y/L119F
Residues in most favoured regions (%)	96.0	94.8	95.6	96.4	94.4	94.0	93.7
Residues in additional allowed regions (%)	4.0	5.2	4.2	3.6	5.6	6.0	6.3
Residues in generously allowed regions (%)	0.0	0.0	0.0	0.0	0.0	0.0	0.0
Residues in disallowed regions (%)	0.0	0.0	0.0	0.0	0.0	0.0	0.0

As defined by PROCHECK.<sup>26</sup>

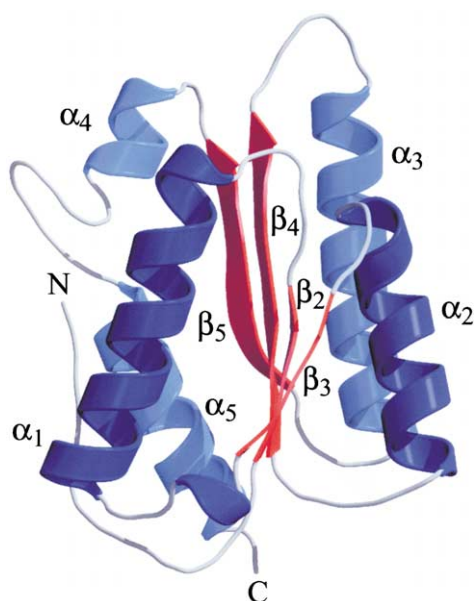


**Figure 4.** Secondary structure arrangement of one *S. pombe* lumazine synthase monomer labelled according to the convention of the *B. subtilis* enzyme.<sup>9</sup> Structure elements are coloured:  $\alpha$ -helix (blue) and  $\beta$ -sheets (red).

### Structural overview and pentamer assembly

All known crystal structures of lumazine synthases from different organisms exhibit a three-layered structure ( $\alpha/\beta/\alpha$ ) which classifies them as  $\alpha\beta$  proteins (Figure 4). The core of the monomer is reminiscent of the flavodoxin fold and consists of a central parallel  $\beta$ -sheet of four strands with topology  $\beta_2\beta_3\beta_4\beta_5$  that is flanked on both sides by the  $\alpha$ -helix motifs  $\alpha_1\alpha_4\alpha_5$  and  $\alpha_2\alpha_3$ ,

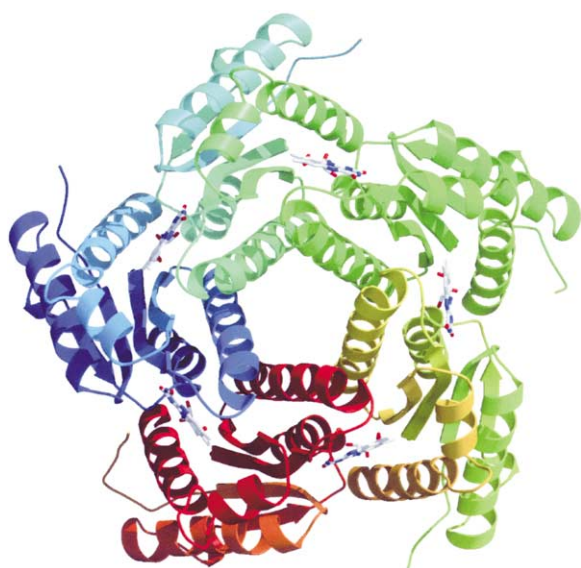


**Figure 5.** Pentameric assembly of *S. pombe* lumazine synthase viewed along the 5-fold non-crystallographic symmetry axis. The active sites are built up by two adjacent monomers. Bound riboflavin is shown in ball-and-stick.

respectively. In accordance with the secondary structure and topology of the *B. subtilis* lumazine synthase,<sup>9</sup> *S. pombe* lumazine synthase is described as  $\beta_2\alpha_1\beta_3\alpha_2\beta_4\alpha_3\beta_5\alpha_4\alpha_5$ . The monomers of various lumazine synthases can be superimposed with r.m.s.d. values between 0.67 and 1.01 Å between 142  $\alpha$ -carbon atoms; this reflects their structural similarity (Figure 7).

Lumazine synthases occur either as pentamers or as icosahedral capsids that are best described as dodecamers of pentamers. The enzymes from *B. subtilis*<sup>9,12</sup> (PDB entry 1RVV), *E. coli*<sup>14</sup> and spinach<sup>15</sup> (PDB entry 1C2Y) form icosahedral capsids of 60 identical  $\beta$ -subunits, whereas the lumazine synthases of *S. pombe*, *S. cerevisiae*<sup>16</sup> (PDB 1EJB), *M. grisea*<sup>15</sup> (PDB 1C41) and *B. abortus*<sup>17</sup> (PDB 1DIO) only assemble to homopentamers.

A main pentamer contact of the *S. pombe* lumazine synthase is provided by the inner helices  $\alpha_3$  of the monomers that are arranged as a superhelical left-handed coiled coil along the 5-fold axis. The interior of the resulting central pore is mainly hydrophilic due to the presence of the residues Glu100, Asp112, Arg108 and His104 of each monomer. The smallest diameter is 6.3 Å measured between the five inner histidine residues His104 which are found in multiple conformations. Salt bridges between Asp112 of one monomer and Arg108 of the neighbouring monomer stabilise the pentamer of *S. pombe* lumazine synthase.

Superposition of the different lumazine synthases reveals some determinants that prevent the formation of icosahedral capsids from pentamers in some organisms. The most prominent differences are located in the loop connecting the helices  $\alpha_4$  and  $\alpha_5$  and in the N termini of the proteins (Figure 7). In all icosahedral structures of bacteria<sup>9,14</sup> and plants<sup>15,22</sup> this loop comprises the highly conserved motif G(T/G)K(A/H)GN which forms a pronounced kink and establishes multiple contacts to helix  $\alpha_1$  and helix  $\alpha_4$  of the adjacent pentamer. It seems likely that the insertion of four residues present in this loop of the *S. cerevisiae* lumazine synthase<sup>16</sup> (GIDEA HSMHN) disrupts contacts to neighbouring subunits and therefore prevents capsid formation. We assume that the insertion of only one residue (Leu136) into this loop (GLNGGHN) is sufficient to prevent capsid formation of lumazine synthase from *S. pombe*.

Note should be taken of the fact that an insertion of amino acids in the sequence of *B. abortus* does not form a clashing kink, but a continuous helix, which does not establish multiple contacts to adjacent pentamers.<sup>17</sup> Therefore the enzyme from *B. abortus* is also unable to form a capsid.

In the icosahedral lumazine synthase crystal structures<sup>9,11,15</sup> the N terminus seems to play an important role in pentamer formation by interacting as the fifth strand  $\beta_1$  of the central  $\beta$ -sheet of the adjacent monomer. The 11 N terminal residues in the *S. pombe* lumazine synthase structure exhibit weak electron density but appear to adopt different conformations in various subunits

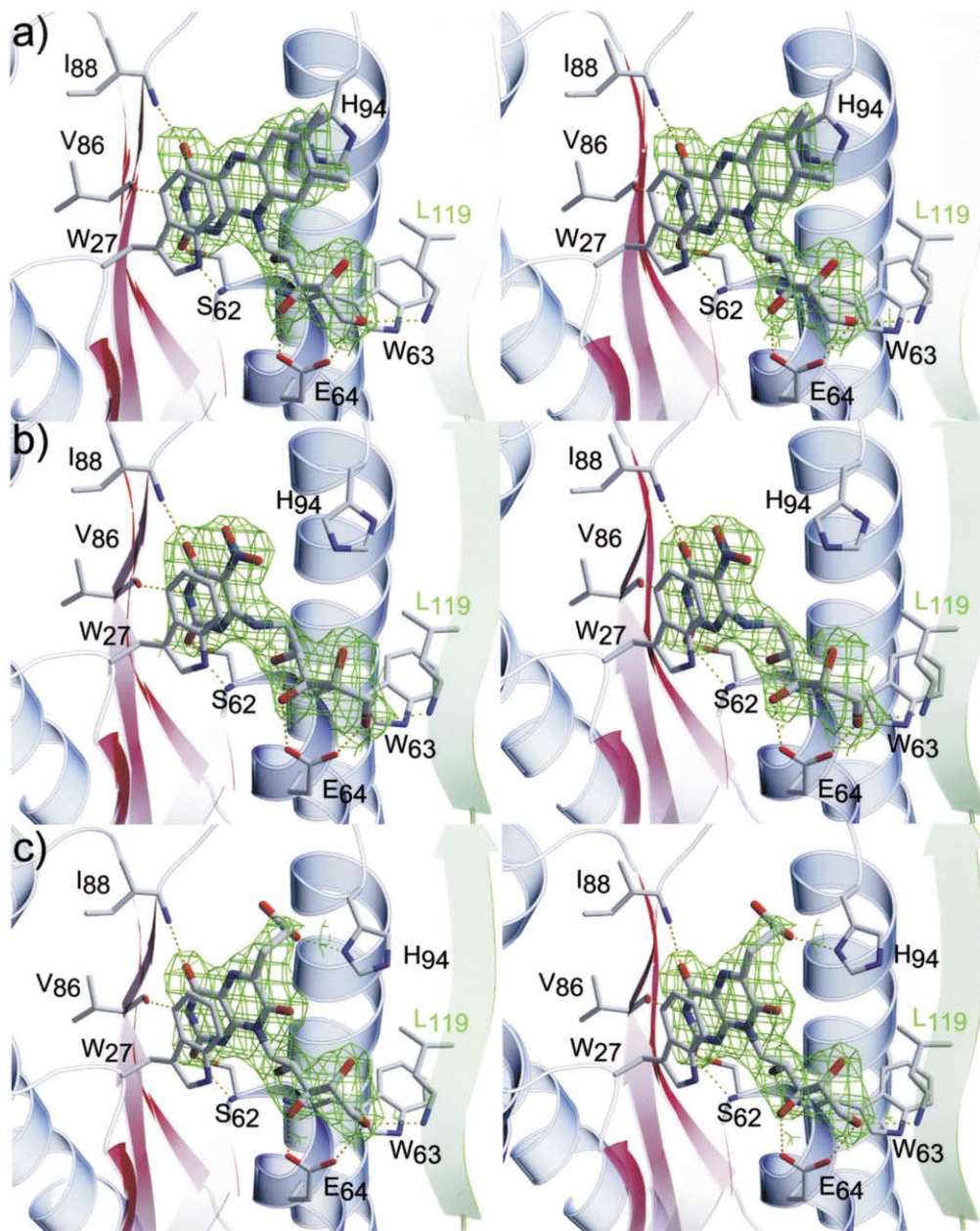


**Figure 6.** Stereo drawings of the substrate binding site of lumazine synthase from *S. pombe*. (a) Bound riboflavin. (b) Substrate analogue inhibitor 5-nitro-6-(D-ribitylamino)-2,4(1H,3H)-pyrimidinedione (8). (c) Product analogue inhibitor 6-carboxyethyl-7-oxo-8-ribityllumazine (9). The final  $2F_o - F_c$  electron density maps covering the bound molecules are contoured at  $1.2\sigma$ . Protein residues from the neighbouring subunit are shown in green.

of the asymmetric pentamer. It can be ruled out that they were proteolytically removed since electrospray mass spectroscopy experiments demonstrated a homogeneous full-length protein.<sup>21</sup>

In the pentameric assembly of the *S. cerevisiae* enzyme,<sup>16</sup> the N-terminal residues play a minor role, as up to 17 residues can be deleted with minor effect on stability of the pentamer assembly and enzymatic activity. N-terminal sequence alignments indicate that proline residues among the first ten residues prevent icosahedral assembly (Figure 8). In the described bacterial<sup>9,11</sup> and plant<sup>15</sup> structures no proline residues are present in this region, whereas in the pentameric structure of

*S. pombe* lumazine synthase two proline residues are found in positions 8 and 10. This conformational arrangement is able to obstruct the introduction of the missing  $\beta_1$ -strand into the neighbouring monomer. However, the N-terminal residues 7–12 of one subunit of the wild-type enzyme point towards the turn between  $\beta_4$  and  $\alpha_3$  of the neighbouring subunit. Therefore Pro8 is very close to the active site residue Trp27 of this subunit and occupies the opposite cleft of the substrate binding site. The presence of proline residues at positions 8 and 10 might be responsible for this conformational arrangement of the N-terminal strand.

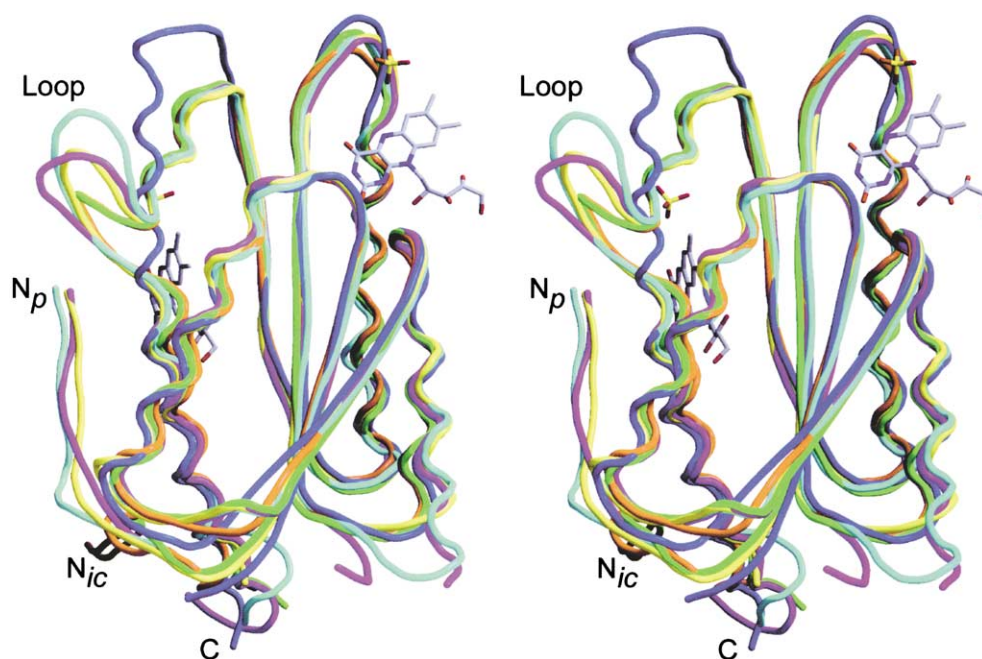


**Figure 7.** Structural superposition of monomers of various lumazine synthases. Enzymes from *S. pombe* (yellow), *B. abortus*<sup>17</sup> (dark blue), *S. cerevisiae*<sup>16</sup> (light blue), and *M. grisea*<sup>15</sup> (magenta) are pentameric, whereas lumazine synthases from *B. subtilis*<sup>9,11</sup> (green), and spinach<sup>15</sup> (orange) form icosahedral capsids. Increase of length of the loop connecting the helices  $\alpha_4$  and  $\alpha_5$  is in accordance with a different orientation of N termini for species forming a capsid ( $N_{ic}$ ) or a pentamer ( $N_p$ ) structure. Bound riboflavin and phosphate ion are shown to mark the substrate binding site and the putative binding site of *S. pombe* lumazine synthase.

### Binding of riboflavin

The five topologically equivalent active sites of the pentameric lumazine synthases are located at the interfaces between adjacent monomers of the pentamer (Figure 5). Here, two substrates have to be bound: 3,4-dihydroxy-2-butanone 4-phosphate (2) and 5-amino-6-(D-ribitylamino)-2,4(1*H*,3*H*)-pyrimidinedione (1) (see Figure 1). The binding site for the latter compound 1 is well-established by complexes of the *B. subtilis*,<sup>12</sup> the spinach and the *M. grisea* lumazine synthases<sup>15</sup> with the inhibitor 5-nitro-6-(D-ribitylamino)-2,4(1*H*,3*H*)-pyrimidinedione (8) (see Figure 3) and of the *S. cerevisiae* lumazine synthase with 5-(6-D-ribitylamino-2,4-dihydroxypyrimidine-5-yl)-1-pentyl-phosphonic acid.<sup>16</sup>

The enzyme from *S. pombe* was the first described lumazine synthase that was found to bind riboflavin with relatively high affinity ( $K_D$  of 1.2  $\mu$ M).<sup>21</sup> Riboflavin is the product of the following enzyme, riboflavin synthase, in the pathway. The position and conformational orientation of bound riboflavin is similar to already known complex structures with substrate analogues. Comparing lumazine synthase crystal structures of either the isolated or the inhibitor-bound proteins from *B. subtilis*,<sup>11</sup> *M. grisea*, spinach,<sup>15</sup> and *S. cerevisiae*<sup>16</sup> with the crystal structure from *S. pombe*, clearly show that riboflavin would act as a competitive inhibitor that binds in the same manner as the inhibitors of the other enzymes. A

bound phosphate ion observed in the structure of *B. subtilis* lumazine synthase<sup>11</sup> has been postulated to mark the phosphate binding site of the second substrate of the enzyme, 3,4-dihydroxy-2-butanone 4-phosphate. This was supported by the *S. cerevisiae* structure with 5-(6-D-ribitylamino-2,4-dihydroxypyrimidine-5-yl)-1-pentyl-phosphonic acid.<sup>16</sup> The phosphonate group of this compound is found in a similar position to the inorganic phosphate ion interacting with the guanidinium group of the highly conserved Arg136. In our structure of *S. pombe* lumazine synthase, an inorganic phosphate ion is found in a similar position, bound to the corresponding residue Arg133.

As mentioned above, the active site is formed at the interface of two adjacent monomers. Monomer A contributes with residues between  $\beta_2$  and  $\alpha_1$ , the turn connecting  $\beta_3$  and  $\alpha_2$  and the strand  $\beta_4$  and helix  $\alpha_3$ . Monomer B takes part with residues from strand  $\beta_5$ , helix  $\alpha_4$  and helix  $\alpha_5$  (Figures 4 and 7). The isoalloxazine ring of the riboflavin molecule is bound to a hydrophobic pocket formed by Trp27, Val86, Leu87, Ile88 and His94 (Figure 6). Polar groups of the riboflavin ring form several hydrogen bonds to main-chain and side-chain atoms of the protein. The carbonyl oxygen of Val86 interacts with the imido group N3 of the ring system. Further interactions are observed between the ring-carbonyl-oxygens atoms O2 and Ser62-N, O4 and Ile88-N and O2 and Ser62-O $\gamma$ .

In all sequences of lumazine synthase either the aromatic residues tryptophan (like *S. pombe*) or



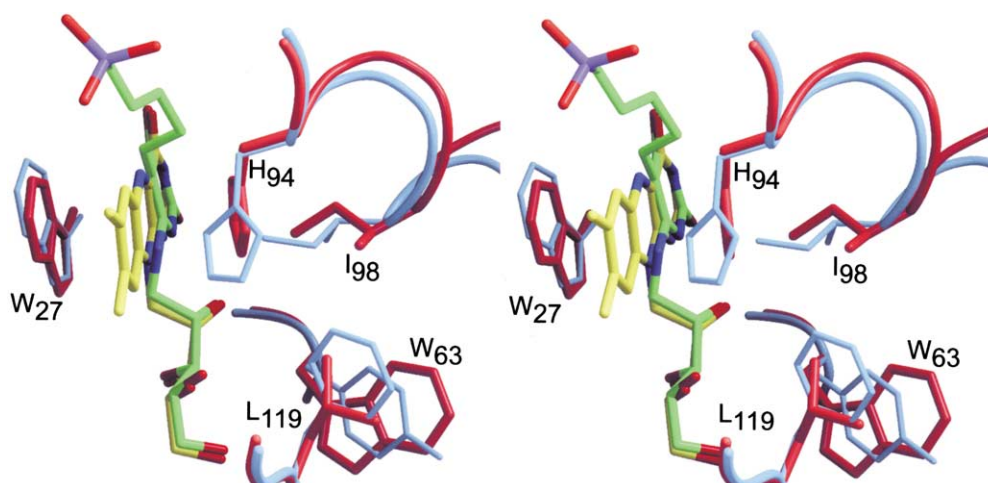


**Figure 9.** Stereo view of superposition of the active site residues formed by two adjacent monomers of the yeast lumazine synthases from *S. pombe* (red) and *S. cerevisiae*<sup>16</sup> (blue). Bound riboflavin (yellow) in case of the *S. pombe* enzyme is in almost the same position as the bound inhibitor 5-(6-D-ribitylamino-2,4-dihydropyrimidine-5-yl)-1-pentyl-phosphonic acid (green) in case of *S. cerevisiae*. Numbers refer to amino acid residues from *S. pombe* lumazine synthase.

phenylalanine (like *B. subtilis*) are found in a position corresponding to Phe22 of the *B. subtilis* enzyme (Figure 8). This suggests the importance of an aromatic stacking interaction for substrate binding. Surprisingly, replacement of Trp27 by glycine substantially reduced the affinity of the *S. pombe* lumazine synthase for riboflavin but had only minor impact on the maximum catalytic rate of the enzyme.<sup>21</sup>

The isoalloxazine ring of riboflavin bound to *S. pombe* lumazine synthase is involved in two aromatic stacking interactions. The indole system of Trp27 is parallel to the ring system at a distance about 3.4 Å. His94 is located at the opposite side of riboflavin about 3.2 Å away building up the second stacking ring (Figure 6(a)). Thus riboflavin is bound by an aromatic “sandwich-packing” between these two aromatic heterocyclic ring systems. The active site residues equivalent to lumazine synthase from *S. pombe* Trp27 and His94 are present in the *M. grisea* (Trp25, His127) and in the *S. cerevisiae* (Trp26, His97) structure with bound substrate analogue, but the capability to bind riboflavin has not been investigated so far.<sup>16</sup> The *B. abortus* sequence also contains this aromatic tryptophan residue (Trp20) but the histidine residue at position 88 is replaced by an arginine and the histidine involved in the binding is found at position 89. This creates a longer distance to a bound substrate or inhibitor molecule.<sup>17</sup> Usually, a high degree of mobility of His88 is observed in the *B. subtilis* binding site.<sup>12</sup>

The ribityl side-chain of bound riboflavin is placed in a hydrophilic pocket of the neighbouring monomers. The ribityl hydroxyl groups OH3 and OH5 are in hydrogen bond distances to the highly conserved residue Glu64. The OH2 ribityl hydroxyl group is hydrogen bonded to the main-chain

amide group of Trp63 of the adjacent monomer. OH5 is also hydrogen bonded to the main-chain amide group and OH4 to a carbonyl oxygen of Leu119 of the second monomer.

#### Binding of a substrate analogue inhibitor

The inhibitor molecule 5-nitro-6-(D-ribitylamino)-2,4(1*H*,3*H*)-pyrimidinedione (8), which is a structural analogue of the natural substrate 1, competes with the riboflavin molecule for the same binding pocket (Figure 6(b)). The pyrimidine ring of 8 is bound in the same way in a hydrophobic region formed by Trp27, Val86, Leu87, Ile88 and the ribityl chain also points to the same hydrophilic environment (Trp63, Glu64, Leu119).

The pyrimidine ring of 8 is in a stacking arrangement with Trp27 at a distance of 3.5 Å. The peptide amide groups of Ser62 and Ile88 are directed towards the O2 and O4 carbonyl groups of the ligand pyrimidine. The main-chain oxygen atom of Val86 is strongly linked to the N3-amide atom of the pyrimidine inhibitor. The side-chain oxygen of Ser62 is involved in additional hydrophilic interaction to the O2 carbonyl. The ribityl hydroxyl groups OH2 and OH5 are hydrogen bonded to main-chain amide groups of Trp63 and Leu119 of the neighbouring monomer, while the well-ordered side-chain Glu64 is involved in two hydrogen bonds to the hydroxyl groups OH3 and OH5. A different stereochemical conformation of the ribityl chain as found in arabityl or xylityl derivatives abolishes the optimal arrangement for the link to Glu64.<sup>12</sup>

A tightly bound inorganic phosphate ion in the 3,4-dihydroxy-2-butanone 4-phosphate binding site was found to be well-defined in the final electron density map. This phosphate is found at a

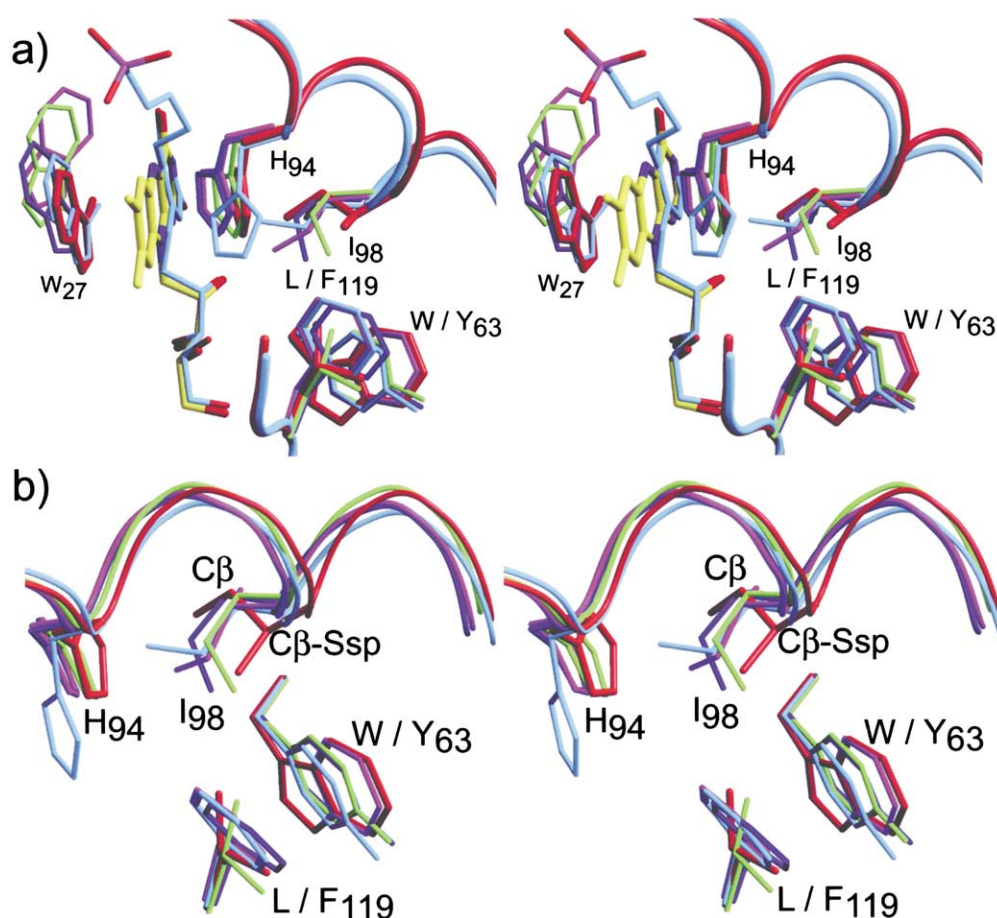


**Figure 10.** (a) Stereo view of the active site residues formed by two adjacent lumazine synthase monomers of *S. pombe* (red) with bound riboflavin (yellow), *S. cerevisiae*<sup>16</sup> (light blue) with bound inhibitor and the mutant enzymes W63Y (green), L119F (magenta) and W63Y/L119F (dark blue). (b) Close up view of the active site chain position of Ile98 of the point mutants in comparison with wild type enzymes from *S. pombe* and *S. cerevisiae*. Numbers refer to amino acid residues from *S. pombe* lumazine synthase.

distance of 6.2 Å to **8** and is bound by main-chain hydrogen interactions of Ser91 and Thr92 and side-chain interaction of Arg133.

### Binding of a product analogue inhibitor

In addition, we co-crystallised lumazine synthase from *S. pombe* with a derivative of the product **3**, 6-carboxyethyl-7-oxo-8-ribityllumazine (**9**). This tightly bound inhibitor molecule is also well defined in its electron density map at 2.6 Å resolution and it is bound in the same manner as described for bound riboflavin or **8** before (Figure 6(c)). The lumazine ring of **9** is in a stacking interaction with Trp27 at a distance of 3.4 Å. The peptide amide groups of Ser62 and Ile88 are oriented towards the O2 and O4 carbonyl groups of the ligand's lumazine ring at 3.0 Å distance. The main-chain oxygen atom of Val86 is strongly hydrogen bonded to the N3-amide atom of the oxo-lumazine inhibitor at a distance of 2.6 Å. The side chain oxygen  $\gamma$ -O of Ser62 is involved in an additional hydrophilic interaction to the O2 carbonyl group of the lumazine. The binding arrangements of the ribityl chain are exactly the

same as mentioned before for bound riboflavin or **8**.

In comparison with the binding of the substrate analogue inhibitor, where no interaction by the residue His94 is observed, hydrogen bonds to the carboxyethyl substituent at position 6 of the lumazine ring are added. Interactions by His94 are an important feature of binding riboflavin.

### Structural basis of riboflavin binding

The wealth of structural information on lumazine synthases from various organisms makes a detailed comparison possible to get insight into the factors that modulate the affinity for riboflavin binding. The structures of the lumazine synthases from *S. pombe* and *S. cerevisiae* were found to be very similar. All residues that interact directly with riboflavin are identical and in the next shell of amino acids residues they differ only by two residues (Trp63 and Leu119 in case of the *S. pombe* enzyme). A superposition of the C $\alpha$ -positions of Trp27, His94 and Leu119 of *S. pombe* lumazine synthase with the corresponding residues Trp26, His97 and Phe122 of the *S. cerevisiae* enzyme

shows an r.m.s. deviation of only 0.23 Å (Figure 9). The positions of the pyrimidinedione and ribityl moieties of the bound inhibitor 5-(6-D-ribitylamino-2,4-dihydropyrimidine-5-yl)-1-pentylphosphonate and of riboflavin fit almost perfectly. Modelling the of riboflavin as bound to the *S. pombe* enzyme to the *S. cerevisiae* enzyme reveals a steric conflict between His97 and Ile101 (*S. cerevisiae*) as the latter is shifted by about 1.0 Å for C<sup>α</sup>-atoms into the binding site of the xylene ring of riboflavin in the *S. pombe* enzyme (Figure 9). As both residues are well ordered and Ile101 is part of the rigid core of the protein a shift of His97/Ile101 upon riboflavin binding appears rather unlikely. Therefore, the dimethylbenzene moiety has to be accommodated in a slightly different orientation.

The ambient residues of the active site of both enzymes differ only at positions 63 and 119 (*S. pombe*) we assumed that their different side chain volumes account for the observed shift of Ile101 relative to Ile98 in *S. pombe* lumazine synthase. To test this hypothesis, we analysed the crystal structures of the mutants Trp63Tyr, Leu119Phe and the respective double mutant and measured their affinity for riboflavin. The structural analysis of these point mutants and comparisons with *S. pombe* and *S. cerevisiae* lumazine synthase show that the positions of the Ile98/Ile101 cluster in a similar position for all proteins with the exception of the wild-type *S. pombe* protein. Its distinct orientation in turn influences the position of His94/His97 (Figure 10). The C<sup>β</sup>-atoms of the cluster assume a position that corresponds to the C<sup>γ</sup>-atom of *S. pombe* wild-type lumazine synthase. This corresponds to a displacement of 1.0 Å between the C<sup>α</sup>-atoms of *S. pombe* and *S. cerevisiae* lumazine synthase. The displacements between the C<sup>β</sup>-atoms of *S. pombe* wild-type enzyme and *S. cerevisiae* lumazine synthase, W63Y, L119F are 1.3 Å and for W63Y/L119F 1.6 Å.

The Trp63Tyr ( $K_D$  of 5.0 μM) and the double mutant Trp63Tyr/Leu119Phe ( $K_D$  of 4.4 μM) showed decreased affinities, with  $K_D$  values very similar to the *S. cerevisiae* enzyme ( $K_D$  of 3.9 μM) as expected. Correspondingly they did not bind riboflavin during purification and were isolated as colourless proteins. Interestingly, a slightly higher affinity was found for the Leu119Phe mutant ( $K_D$  of 0.3 μM), which showed a faint yellow colour after purification. In that case the additional van der Waals contact between His94 and Phe119 (4.1 Å minimum distance) may account for the slightly increased affinity.

For comparison the affinity of the *B. subtilis* enzyme, a more distant member of the lumazine synthase family, was determined which yielded a  $K_D$  of at least 1 mM. In that enzyme Ile98 is replaced by Val92 accompanied by a shift of the C<sup>α</sup>-positions by 1.5 Å towards the substrate binding site. The C<sup>γ</sup> atom of Val92 is only in contact with one edge of the corresponding His88 and does not support its entire backside. This might

account for the flexibility of His88 of the *B. subtilis* enzyme usually observed and might be seen as a major reason for the largely reduced affinity to riboflavin.

We conclude from our studies that the stacking interaction between riboflavin's xylene ring and His94 is required for efficient binding of riboflavin to lumazine synthase. The structural and functional analysis of wild-type and mutant enzymes revealed small and indirect effects with the most pronounced difference seen in the orientation of the neighbouring Ile98 or the presence of Phe119 that pack against His94. These appear to be sufficient to influence the essential stacking contact and thereby significantly modulate the affinity for riboflavin. At present, it is unknown whether the micro-molar affinity of some lumazine synthases for riboflavin, the ultimate product of the pathway, as observed here, plays a role as feedback regulatory mechanism *in vivo*.

## Materials and Methods

### Expression, purification and crystallisation

The wild-type *S. pombe* lumazine synthase and the mutant protein W27G were cloned, expressed and purified as described by Fischer *et al.*<sup>21</sup> Binding constants were determined by fluorescence titration or by equilibrium dialysis (*B. subtilis*) as described.<sup>21</sup> The cloning, expression and the purification of the mutant proteins W63Y, L119F and W63Y/L119F will be described elsewhere. After purification in the absence of riboflavin an average of 20% of the purified wild-type enzyme had bound the ligand.<sup>21</sup> Therefore, for crystallisation the enzyme solution was saturated with solid riboflavin. Crystallisation was performed by the sitting drop vapour diffusion method by mixing equal amounts of wild-type enzyme (10 mg/ml) containing riboflavin in 20 mM potassium phosphate (pH 7.0) and 50 mM potassium chloride with reservoir solution containing 0.1 M citrate (pH 4.9–5.2) and 1.5 M sodium formate followed by equilibration against 0.3 ml of the reservoir buffer. Dark yellow crystals indicating the binding of riboflavin appeared within one to three days of maximal dimensions 0.4 mm × 0.2 mm × 0.2 mm. Crystals of the mutant enzymes W27G, W63Y, L119F and W63Y/L119F were grown from 0.1 M citrate (pH 5.0–5.6) containing 0.9–1.2 M ammonium dihydrogen phosphate.

Co-crystallisation experiments with substrate analogue 5-nitro-6-(D-ribitylamino)-2,4(1H,3H)-pyrimidinedione and product analogue 6-carboxyethyl-7-oxo-8-ribityllumazine inhibitors were carried out by mixing wild-type enzyme (10 mg/ml) containing riboflavin with solid inhibitors. Sitting drops were set up from 2 μl each of the inhibitor solutions containing tenfold molar excess of the corresponding inhibitor mixed with 2 μl of 0.1 M citrate (pH 5.0–5.5) and 0.3–0.7 M ammonium dihydrogen phosphate at room temperature.

### Data collection

X-ray data for the riboflavin-bound wild-type enzyme, the three mutant enzymes W63Y, L119F, W63Y/L119F and for the two inhibitor complex structures were collected on a MARRResearch 345 imaging plate detector

system mounted on a Rigaku RU-200 rotating anode operated at 50 mA and 100 kV with  $\lambda = \text{Cu K}\alpha = 1.542 \text{ \AA}$ . The native data sets up to 2.4 Å were integrated with MOSFLM.<sup>23</sup> Crystals containing riboflavin belong to the space group C222<sub>1</sub> with cell constants  $a = 111.50 \text{ \AA}$ ,  $b = 145.52 \text{ \AA}$ ,  $c = 128.70 \text{ \AA}$ . The asymmetric unit contained one pentamer resulting in a Matthews coefficient of  $3.04 \text{ \AA}^3/\text{Da}$ .<sup>24</sup> Co-crystals of the inhibitor molecules belonged to the same orthorhombic space group with cell dimensions of  $a = 111.26 \text{ \AA}$ ,  $b = 145.04 \text{ \AA}$ ,  $c = 127.86 \text{ \AA}$  and  $a = 111.09 \text{ \AA}$ ,  $b = 145.18 \text{ \AA}$ ,  $c = 128.55 \text{ \AA}$ , respectively.

For the mutant enzyme W27G a data set to 2.0 Å was measured at the DESY synchrotron source beamline BW6 (Hamburg, Germany) with  $\lambda = 1.05 \text{ \AA}$  at room temperature employing a MARRResearch CCD detector. This colourless crystal form belongs also to the space group C222<sub>1</sub> with the cell constants  $a = 110.57 \text{ \AA}$ ,  $b = 144.02 \text{ \AA}$ ,  $c = 126.36 \text{ \AA}$ .

Images from the MARRResearch CCD detector were processed with the HKL package.<sup>25</sup> All data sets were further processed using programs from the CCP4 suite.<sup>26</sup> Data collection statistics are shown in Table 1.

### Structure solution

The crystal structure of lumazine synthase from *S. pombe* was solved by molecular replacement using the program MOLREP.<sup>26</sup> A pentamer taken from the icosahedral structure of lumazine synthase from *B. subtilis*<sup>12</sup> (PDB entry 1RVV) was used as a Patterson search model. The rotation function calculation was performed between 38 and 4.5 Å. The highest peak was used for translational search, giving a top solution with a correlation coefficient of 37.9%. In the following translation search the highest peak gave the correct solution with correlation coefficient of 14.18 over 8.37 for the first false. The orientations and positions of the mutant pentamers and the two inhibitor enzyme complexes were determined using the finally refined structure of wild-type lumazine synthase from *S. pombe* excluding the co-ordinates for the riboflavin. Examination of the packing of the proteins within the crystal lattice indicated reasonable crystal contacts between the lumazine synthase pentamers without overlap of symmetry-related molecules.

### Model building and refinement

The initial model was subjected to rigid body and positional refinement using CNS.<sup>27</sup> Model building was performed with the program MAIN.<sup>28</sup> After several cycles of manual rebuilding, positional and B-factor refinement and two rounds of simulated annealing, water molecules were incorporated automatically into the various models. Restrained non-crystallographic symmetry of  $40 \text{ kcal mol}^{-1} \text{ \AA}^{-2}$  was applied in all subsequent steps of refinement for each of the *S. pombe* lumazine synthase structures. In later stages of crystallographic refinement, the maximum-likelihood algorithm implemented in the program CNS was used. A geometry check using the program PROCHECK<sup>29</sup> revealed that 96.0% and 4.0% for wild-type (RIBO) and 96.4% and 3.6% for the mutant protein W27G of all non-glycine residues lie within the most favoured and additionally allowed regions of the Ramachandran plot.<sup>30</sup> For the two inhibitor complex structures (CEOL and NRAP) and the additional mutant structures (W63Y, L119F and

W63Y/L119F) the geometry check leads to nearly the same good stereochemistry as for the ligand-free enzyme (see Table 2).

### Analysis and graphical representation

Stereochemical parameters were assessed with PROCHECK.<sup>29</sup> Protein structures were three-dimensional aligned with TOP3D<sup>26</sup> and superpositions further refined with MAIN.<sup>28</sup> Structural Figures. were prepared with MOLSCRIPT,<sup>31</sup> BOBSCRIPT<sup>32</sup> and RASTER3D.<sup>33</sup>

### Acknowledgments

This work was supported by the Deutsche Forschungsgemeinschaft, the Fonds der Chemischen Industrie, the Hans-Fischer-Gesellschaft e.V., the E.C. grant, and by NIH grant GM51469.

### References

1. Neuberger, G. & Bacher, A. (1985). Biosynthesis of riboflavin. An aliphatic intermediate in the formation of 6,7-dimethyl-8-ribityllumazine from pentose phosphate. *Biochem. Biophys. Res. Commun.* **127**, 175–181.
2. Neuberger, G. & Bacher, A. (1986). Biosynthesis of riboflavin. Enzymatic formation of 6,7-dimethyl-8-ribityllumazine by heavy riboflavin synthase from *Bacillus subtilis*. *Biochem. Biophys. Res. Commun.* **139**, 1111–1116.
3. Nielsen, P., Neuberger, G., Floss, H. G. & Bacher, A. (1984). Biosynthesis of riboflavin. Enzymatic formation of the xylene moiety from [14C]ribulose 5-phosphate. *Biochem. Biophys. Res. Commun.* **118**, 814–820.
4. Bacher, A., Le Van, Q., Keller, P. J. & Floss, H. G. (1983). Biosynthesis of riboflavin. Incorporation of 13C-labeled precursors into xylene ring. *J. Biol. Chem.* **258**, 13431–13437.
5. Kis, K., Volk, R. & Bacher, A. (1995). Biosynthesis of riboflavin. Studies on the reaction mechanism of 6,7-dimethyl-8-ribityllumazine synthase. *Biochemistry*, **34**, 2883–2892.
6. Kis, K. & Bacher, A. (1995). Substrate channeling in the lumazine synthase/riboflavin synthase complex of *Bacillus subtilis*. *J. Biol. Chem.* **270**, 16788–16795.
7. Bacher, A., Baur, R., Eggers, U., Harders, H. D., Otto, M. K. & Schnepfle, H. (1980). Riboflavin synthases of *Bacillus subtilis*. Purification and properties. *J. Biol. Chem.* **255**, 632–637.
8. Ladenstein, R., Ludwig, H. C. & Bacher, A. (1983). Crystallization and preliminary X-ray diffraction study of heavy riboflavin synthase from *Bacillus subtilis*. *J. Biol. Chem.* **258**, 11981–11983.
9. Ladenstein, R., Schneider, M., Huber, R., Bartunik, H. D., Wilson, K., Schott, K. & Bacher, A. (1988). Heavy riboflavin synthase from *Bacillus subtilis*. Crystal structure analysis of the icosahedral beta 60 capsid at 3.3 Å resolution. *J. Mol. Biol.* **203**, 1045–1070.
10. Bacher, A., Ludwig, H. C., Schnepfle, H. & Ben-Shaul, Y. (1986). Heavy riboflavin synthase from *Bacillus subtilis*. Quaternary structure and reagggregation. *J. Mol. Biol.* **187**, 75–86.

11. Ladenstein, R., Ritsert, K., Huber, R., Richter, G. & Bacher, A. (1994). The lumazine synthase/riboflavin synthase complex of *Bacillus subtilis*. X-ray structure analysis of hollow reconstituted beta-subunit capsids. *Eur. J. Biochem.* **223**, 1007–1017.
12. Ritsert, K., Huber, R., Turk, D., Ladenstein, R., Schmidt-Bäse, K. & Bacher, A. (1995). Studies on the lumazine synthase/riboflavin synthase complex of *Bacillus subtilis*: crystal structure analysis of reconstituted  $\beta$ -subunit capsids with bound substrate analogue inhibitor at 2.4 Å resolution. *J. Mol. Biol.* **253**, 151–167.
13. Zhang, X., Meining, W., Fischer, M., Bacher, A. & Ladenstein, R. (2001). X-ray structure analysis and crystallographic refinement of lumazine synthase from the hyperthermophile *Aquifex aeolicus* at 1.6 Å resolution: determinants of thermostability revealed from structural comparisons. *J. Mol. Biol.* **306**, 1099–1114.
14. Mörtl, S., Fischer, M., Richter, G., Tack, J., Weinkauff, S. & Adelbert, A. (1996). Biosynthesis of riboflavin. Lumazine synthase of *Escherichia coli*. *J. Biol. Chem.* **271**, 33201–33207.
15. Persson, K., Schneider, G., Jordan, D. N., Viitanen, P. V. & Sandalova, T. (1999). Crystal structure analysis of a pentameric fungal and an icosahedral plant lumazine synthase reveals the structural basis for differences in assembly. *Protein Sci.* **8**, 2355–2365.
16. Meining, W., Mörtl, S., Fischer, M., Cushman, M., Bacher, A. & Ladenstein, R. (2000). The atomic structure of pentameric lumazine synthase from *Saccharomyces cerevisiae* at 1.85 Å resolution reveals the binding mode of a phosphonate intermediate analogue. *J. Mol. Biol.* **299**, 181–197.
17. Braden, B. C., Velikovskiy, C. A., Cauerhff, A. A., Polikarpov, I. & Goldbaum, F. A. (2000). Divergence in macromolecular assembly: X-ray crystallographic structure analysis of lumazine synthase from *Brucella abortus*. *J. Mol. Biol.* **297**, 1031–1036.
18. Shavlovskiy, G. M., Teslyar, G. E. & Strugovshchikova, L. P. (1982). Regulation of flavogenesis in riboflavin-dependent *Escherichia coli* mutants. *Mikrobiologiya*, **51**, 986–992.
19. Shavlovskiy, G. M., Sibirny, A. A., Kshanovskaya, B. V., Koltun, L. V. & Logvinenko, E. M. (1979). Genetic classification of riboflavinless mutants of *Pichia guilliermondii* yeast. *Genetika (Moscow)*, **15**, 1561–1568.
20. Oltmanns, O., Bacher, A., Lingens, F. & Zimmermann, F. K. (1969). Biochemical and genetic classification of riboflavin deficient mutants of *Saccharomyces cerevisiae*. *Mol. Gen. Genet.* **105**, 306–313.
21. Fischer, M., Haase, I., Feicht, R., Richter, G., Gerhardt, S., Changeux, J.-P. *et al* (2002). Biosynthesis of riboflavin. 6,7-Dimethyl-8-ribityllumazine synthase of *Schizosaccharomyces pombe*. *Eur. J. Biochem.* **269**, 519–526.
22. Jordan, D. B., Bacot, K. O., Carlson, T. J., Kessel, M. & Viitanen, P. V. (1999). Plant riboflavin biosynthesis. Cloning, chloroplast location, expression, purification, expression, and partial characterization of spinach lumazine synthase. *J. Biol. Chem.* **274**, 22114–22121.
23. Leslie, A.G.W. (1998). MOSFLM 6.0 edit. Cambridge, UK
24. Matthews, B. W. (1968). Solvent content of protein crystals. *J. Mol. Biol.* **33**, 491–497.
25. Otwinowski, Z. & Minor, W. (1997). Processing of X-ray diffraction data collected in oscillations mode. *Methods Enzymol.* **276**, 307–326.
26. Collaborative Computational Project, N (1994). The CCP4 Suite: programs for protein crystallography. *Acta Crystallog. sect. D*, **50**, 760–763.
27. Brünger, A. T. *et al.* (1998). Crystallography and NMR system (CNS): a new software system for macromolecular structure determination. *Acta Crystallog. sect. D*, **54**, 905–921.
28. Turk, D. (1992). Weiterentwicklung eines Programmes für Molekülgraphik und Elektronendichte-Manipulation und seine Anwendung auf verschiedene Protein-Strukturaufklärungen. PhD Thesis. Technische Universität München, München
29. Laskowski, R. A., MacArthur, M. W., Moss, D. S. & Thornton, J. M. (1993). PROCHECK: a program to check the stereochemical quality of protein structures. *J. Appl. Crystallog.* **26**, 283–291.
30. Ramachandran, G. N. & Sasisekharan, V. (1968). Conformation of polypeptides and proteins. *Advan. Protein Chem.* **23**, 283–437.
31. Kraulis, P. J. (1991). MOLSCRIPT: a program to produce both detailed and schematic plots of protein structures. *J. Appl. Crystallog.* **24**, 946–950.
32. Esnouf, R. M. (1997). An extensively modified version of MolScript that includes greatly enhanced coloring capabilities. *J. Mol. Graph. Model.* **15**, 112–113. see also pp. 132–134.
33. Merritt, E. A. & Murphy, M. E. P. (1994). Raster3D Version 2.0. A program for photorealistic molecular graphics. *Acta Crystallog. sect. D*, **50**, 869–873.
34. Barton, G. J. (1993). ALSRIPT: a tool to format multiple sequences alignments. *Protein Eng.* **6**, 37–40.

Edited by D. Rees

(Received 2 October 2001; received in revised form 25 January 2002; accepted 26 January 2002)